This article has been accepted for publication in a future issue of this journal, but has not been fully edited. Content may change prior to final publication. Citation information: DOI 10.1109/TSTE.2019.2932613, IEEE Transactions on Sustainable Energy

Transient Stability Analysis and Enhancement of Renewable Energy Conversion System During LVRT

Xiuqiang He, *Student Member, IEEE*, Hua Geng, *Senior Member, IEEE*, Ruiqi Li, and Bikash Chandra Pal, *Fellow, IEEE*

***Abstract*—Grid-connected renewable energy conversion systems (RECSs) are usually required by grid codes to possess the low voltage ride through (LVRT) and reactive power support capabilities so as to cope with grid voltage sags. During LVRT, RECS's terminal voltage becomes sensitive and changeable with its output current, which brings a great challenge for the RECS to resynchronize with the grid by means of phase-locked loops (PLLs). This paper indicates that loss of synchronism (LOS) of PLLs is responsible for the transient instability of grid-connected RECSs during LVRT, and the LOS is essentially due to the transient interaction between the PLL and the weak terminal voltage. For achieving a quantitative analysis, an equivalent swing equation model is developed to describe the transient interaction. Based on the model, the transient instability mechanism of RECSs during LVRT is clarified. Furthermore, a transient stability enhancement method is proposed to avoid the possibility of transient instability. Simulations performed on the New England 39-bus test system verify the effectiveness of the method.**

***Index Terms*—Renewable energy conversion system, grid faults, low voltage ride through, transient stability, power converter.**

I. Introduction

GRID-CONNECTED renewable energy conversion systems (RECSs), such as wind energy conversion systems (WECSs) and photovoltaic (PV) generation systems, have become an important part of the power system. RECSs present quite different characteristics from conventional synchronous generators (SGs). By employing power converters, RECSs provide faster power response but more limited fault tolerant capability than SGs while subjected to grid faults [1].

For the steady-state and transient performance of RECSs after grid faults occur, three successive stages are characterized in low voltage ride through (LVRT) studies [2]–[4].

1) *Stage I is the first several cycles after grid faults*, in which protection or control countermeasures are taken to stand the impact of transients in order to protect converters from damage. 2) *Stage II is the low-voltage-sustaining stage*, in which the RECS's resynchronization with the grid must be achieved as soon as possible, and the control function of power converter should be regained to support the grid voltage by supplying some reactive current, according to specifications from grid codes [5]. For example, RECSs are required to output 100% reactive current when the voltage at the point of common coupling (PCC) dips below 50% [5]. RECSs are allowed to trip off if the PCC voltage is below the specified voltage profile [5]. 3) *Stage III is the voltage recovery stage after the fault clearance*, in which the reactive current injection is withdrawn and the active power supply is restored gradually.

The LVRT capability, protection and control strategies in the Stage I and Stage II have been extensively investigated in prior studies [2]–[4]. However, these studies are mainly focused on electromagnetic transient analysis of doubly-fed induction generator (DFIG) after grid voltage dips, as well as enhancements of the LVRT capability. In these studies, the RECS terminal voltage dynamics during grid faults are neglected. In other words, the terminal voltage is deemed constant or unchanged, which is reasonable in stiff grid scenarios, but not so for weak grid. In fact, the post-fault equivalent grid impedance becomes considerable in weak grid and it makes the RECS terminal voltage very responsive to the output current/power of the RECS. The terminal voltage is then used as input to the phase-locked loop (PLL) to estimate the phase-angle and frequency of the power grid. Owing to the interaction between the terminal voltage and the PLL output, it is difficult for the RECS to achieve resynchronization with the power grid.

For the *small-signal stability* of PLL-synchronized RECSs during riding through symmetrical or asymmetrical faults, numerous studies such as [6]–[9] have been conducted using eigenvalue analysis and impedance analysis based on the small-signal model. The findings have indicated that weak grid connection is able to deteriorate the small-signal stability. Besides, improper PLL parameters are proved to have negative impacts on the stability in terms of resynchronization with the power grid [6]–[9]. However, the small-signal stability analyses are only effective in the neighborhood of the specific steady-state point rather than the full state space.

In the last few years, *large-signal stability* issues of RECSs are attracting increasing attention [10]–[24]. Göksu *et al*. and Dong *et al*. made pioneering contributions in [11] and [12], respectively. Reference [11] investigated RECS's loss of synchronism (LOS) with the grid during deep voltage sags and proposed a stability criterion focused on the existence of equilibrium points. Reference [12] gave deep insights into low-frequency nonlinear behaviors of PLLs and proposed an equivalent criterion to that in [11]. However, a RECS satisfying the criterion [11], [12] may still lose synchronism due to improper initial states or poor transient properties, as found in our prior work [13]–[16]. In [13]–[16], we revealed that the tran-

This work was supported by National Natural Science Foundation of China (NSFC) under Grant 61722307, Grant U1510208. Paper no. TSTE-00206-2019. *(Corresponding author: Hua Geng.)*

X. He and H. Geng are with Beijing National Research Center for Information Science and Technology, Department of Automation, Tsinghua University, Beijing 100084, China (e-mail: he-xq16@mails.tsinghua.edu.cn; genghua@tsinghua.edu.cn).

R. Li is with the China Electronics Standardization Institute, Beijing 100007, China (e-mail: lirq@cesi.cn).

B. C. Pal is with the Department of Electrical and Electronic Engineering, Imperial College, London SW7 2AZ, U.K. (e-mail: b.pal@imperial.ac.uk).

This article has been accepted for publication in a future issue of this journal, but has not been fully edited. Content may change prior to final publication. Citation information: DOI 10.1109/TSTE.2019.2932613, IEEE Transactions on Sustainable Energy

sient stability is related to the existence of equilibrium points, initial states, and system transient properties. Recently, X. Wang's research group [17]–[20] created a new perspective by using the phase portrait method to analyze the transient stability of grid-connected converters, though the method has high complexity and low physical insight [20]. Besides, the Lyapunov's direct method have also been applied to investigate the transient stability of voltage-controlled grid-connected converters [21], [22]. However, it is still an unresolved problem to develop a proper Lyapunov function candidate specially for assessing the transient stability of PLL-synchronized current-controlled converters [20].

The transient stability of conventional power systems (often referred as to the rotor-angle stability) has been widely studied. Based on the rotor swing equation and neglecting the system damping, the equal area criterion (EAC) is easily employed to assess the rotor-angle stability. Although various "swing equations" of grid-connected power converters have been developed previously [25], [26] to investigate the capability of power converter to mimic the inertia and frequency support characteristics of SGs, the "swing equation" concept together with the EAC method was rarely used to study the transient stability of PLL-synchronized converters. References [23], [24] made such innovative attempts. Actually, the EAC method is a special case of the Lyapunov's direct method [20]. Without considering the system damping, the EAC method is quite easy to use and it has high physical insight to understand the underlying mechanism of the transient instability. In addition, quantitative criteria that are simple and convenient for stability judgements can be drawn from the EAC method, although the criteria are relatively conservative since the system damping is neglected [20].

When it comes to the transient stability enhancement, it is noticed that the prior arts [10], [11], [13] are inadequate because of various defects, as summarized in [20]. For example, the PLL freezing method [11] cannot address grid phase jumps; the adaptive current injecting method [13] requires to estimate the network impedance X/R ratio. Therefore, other alternatives to enhance the transient stability need to be further explored.

This paper continues our research [13]–[16]. The particular attention is focused on the quantitative criterion and enhancement method of the transient stability of RECSs. A novel "swing equation" describing the transients after grid voltage sags is developed in Section II. It indicates that the transient stability is affected by the interaction between the PLL and the terminal voltage, and the interaction is also involved with the active power control (APC). Basically, the transient stability within the LVRT Stage II can be maintained as long as an appropriate active power reference is given. A quantitative stability analysis is performed in Section III, yielding the quantitative stability criterion. Also, a transient stability enhancement method based on dynamic active power balance, by means of automatically regulating the active power reference to improve the transient stability, is developed in Section IV. Section V verifies the effectiveness of the method. By comparison with three state-of-the-art methods, the proposed method shows high performance while maintaining the transient stability.

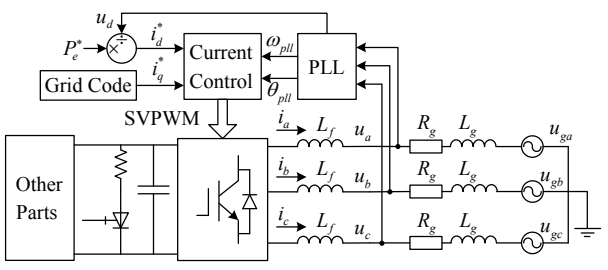

Fig. 1. An SMIB system embodying a simplified RECS, where P_e^* during LVRT is typically set to zero [11], [13]. Note this study takes full-scale power converter based RECSs as an example in analyzing the transient stability. The modeling and analysis methods are also applicable to type III WECSs [13].

II. System Modelling

A typical diagram of the power grid integrated with a single capability-rescaled RECS is shown in Fig. 1. The "Other Parts" of the RECS is equivalent to a constant DC voltage source during the LVRT Stage II considering that the utilized protective measures such as chopper circuit can maintain the DC-link voltage [13]–[20]. The power grid is represented by a Thévenin equivalent circuit with voltage amplitude U_g and frequency ω_g. The entire system is considered as a single-machine infinite-bus (SMIB) system. In Fig. 1, u_x is the terminal voltage of the RECS, i_x is the output current of the RECS and $x = a, b, c$; R_g and L_g are the resistor and inductor of the equivalent grid impedance, respectively; ω_{pll} and θ_{pll} are the frequency and phase angle detected by the PLL, respectively. Note that all these variables are expressed in the per unit system where time is measured in seconds.

A. Reduced-Order Nonlinear Model

Both current control dynamics and electromagnetic transients of the terminal filter (not depicted in Fig. 1) can be ignored while analyzing the nonlinear PLL dynamics [13]–[20], since the bandwidth of the current control loop with appropriate parameters is much higher than that of the PLL. Consequently, the RECS during LVRT can be regarded as a controlled current source [13]–[20]. The output current of the RECS is denoted as $i_d \approx i_d^*$ and $i_q \approx i_q^*$, where i_q^* is specified by grid codes during grid faults, e.g., $i_q^* = -1.0$ p.u. [5], and i_d^* could be given by the active power control (APC) loop,

$$i_d^* = P_e^* / u_d \tag{1}$$

where P_e^* denotes the active power reference. Note that grid codes have not yet specified that RECSs have to perform active current injection during LVRT [13] and hence P_e^* is typically set to zero during LVRT in view of capacity limit of converters.

A typical PLL diagram is shown in Fig. 2(a), which is widely utilized for symmetrical grid conditions. The frequency base ω_b in the per unit system is taken as the rated nominal frequency. The PLL model is given by

$$\begin{cases} d\theta_{pll}/dt = \omega_b \omega_{pll} \\ d\left(\omega_b \omega_{pll}\right)/dt = k_p\, du_q/dt + k_i u_q. \end{cases} \tag{2}$$

The gain parameters k_p and k_i are crucial to shape the dynamics of the PLL. On the choices of k_p and k_i as well as the

This article has been accepted for publication in a future issue of this journal, but has not been fully edited. Content may change prior to final publication. Citation information: DOI 10.1109/TSTE.2019.2932613, IEEE Transactions on Sustainable Energy

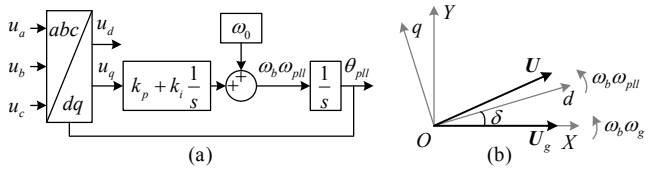

Fig. 2. (a) Typical synchronous reference frame PLL (SRF-PLL), where ω_0 is the nominal frequency such as 100π. (b) Relationship between the PLL reference frame and the infinity bus reference frame.

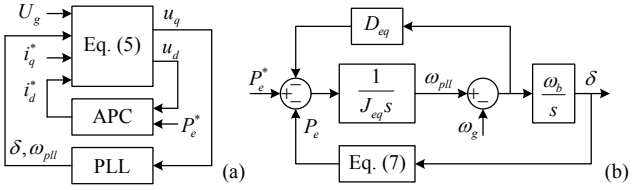

Fig. 3. Diagram of the system model. (a) Interaction illustration. (b) Equivalent swing equation to (a). Note that the swing equation developed here is intended for transient stability studies, distinct from existing ones in [25] and [26] used to study inertia imitation in frequency regulation.

bandwidth of the PLL, a guideline is offered in Appendix.

The PLL reference frame [i.e., *dq* reference frame in Fig. 2(b)] and the infinity bus synchronous reference frame [i.e., *XY* reference frame] are rotating with the PLL frequency $\omega_b\omega_{pll}$ and the actual grid frequency $\omega_b\omega_g$, respectively. The included angle δ between these two reference frames is denoted as

$$\delta = \theta_{pll} - \theta_g \tag{3}$$

where θ_{pll} is the absolute angle of the PLL relative to the stationary reference frame; θ_g is the phase angle of the grid voltage vector $\boldsymbol{U}_g$; δ is referred to as the relative angle of the PLL (*PLL angle* for short thereinafter) relative to the *XY* reference frame [see Fig. 2(b)]. Hence, the following expression can be derived,

$$d\delta/dt = \omega_b\left(\omega_{pll} - \omega_g\right). \tag{4}$$

While neglecting the electromagnetic transients of grid impedance, the quasi steady-state model is expressed in the PLL reference frame as follow,

$$\begin{bmatrix} u_d \\ u_q \end{bmatrix} = \begin{bmatrix} \cos\delta & \sin\delta \\ -\sin\delta & \cos\delta \end{bmatrix}\begin{bmatrix} U_g \\ 0 \end{bmatrix} + R_g\begin{bmatrix} i_d \\ i_q \end{bmatrix} + \omega_{pll}L_g\begin{bmatrix} -i_q \\ i_d \end{bmatrix}. \tag{5}$$

The above equations (1)–(5) describe the transient nonlinear behaviors of the system, as illustrated in Fig. 3(a). There is an interaction between the terminal voltage u_q and the PLL output δ. The APC is also involved in the interaction since u_d is used in the APC to calculate the active current reference. Given that the nonlinear model is second-order, it is doable to further transform the model to an equivalent swing equation.

B. Equivalent Swing Equation

Based on (1)–(5), the equivalent swing equation can be derived as (see Appendix for more details),

$$J_{eq}\, d\omega_{pll}/dt = P_e^* - P_e - D_{eq}\left(\omega_{pll} - \omega_g\right) \tag{6}$$

where J_{eq} and D_{eq} denote the equivalent inertial and damping coefficients, respectively; P_e is the actual active power output, which is a function of δ when given P_e^*, i_q^*, and U_g,

$$P_e = u_d i_d + u_q i_q = f\left(\delta\right)\Big|_{P_e^*,\ i_q^*,\ U_g}. \tag{7}$$

The function f can be derived from (1), (5) and (7). It is not shown here as its analytical form is too complex. From (A.10) in Appendix, it is found that J_{eq} can be approximately considered as a constant since its last two terms are far less than 1.0. By contrast, D_{eq} cannot be regarded as a constant since it changes significantly with the PLL angle δ.

Fig. 3(b) depicts the swing equation, which is the same in form as swing equation of a SG. Hence, RECSs share a strong similarity with SGs in terms of mathematical model describing synchronization dynamics during symmetrical grid faults. The synchronization dynamics of SGs are affected by the unbalanced power term. Similarly, the synchronization dynamics of RECSs are affected by the active power deviation ($P_e^* - P_e$). In fact, the motion of the PLL is really driven by its input variable u_q. Equation (A.8) establishes the relationship between u_q and the active power deviation ($P_e^* - P_e$). Therefore, it is understandable that the motion of the PLL can be equivalently driven by ($P_e^* - P_e$), in terms of mathematical analysis.

III. Transient Stability Analysis

The transient stability mechanism and criterion have been preliminarily studied in [11] and [12]. Briefly, after a grid voltage sags, the existence of a new equilibrium point is a prerequisite for the transient stability of the system. But even if the criterion regarding the equilibrium point is met, the system may still become unstable due to poor transient behaviors [13]. Here, it is summarized that the factors affecting the transient stability include two aspects: 1) existence of equilibrium points and 2) system transient properties. The first factor is explained with the steady-state active power output range, and the second factor is explained using the developed swing equation and the easy-to-follow equal area criterion (EAC).

A. Steady-State Active Power Output Range

Equation (6) suggests that P_e^* is equal to P_e while the operating point reaches the equilibrium point. For a RECS during grid fault, there is an allowable range for actual active power output. Hence, an appropriate active power reference, which should be set within the active power output range, is significant for the existence of the equilibrium point.

With a given grid voltage U_g, the active power output range is constrained by the maximum current limit $I_{\max}$ and the reactive current requirement i_q from grid codes. The steady-state active power output range [$P_{e\min}$, $P_{e\max}$] can be solved by,

$$\begin{aligned} \max,\ \min \quad & P_e = u_d i_d \\ \text{s.t.} \quad & U_g\cos\delta + R_g i_d - X_g i_q = u_d \\ & U_g\sin\delta - R_g i_q - X_g i_d = 0 \\ & \sqrt{i_d^2 + i_q^2} \le I_{\max}. \end{aligned} \tag{8}$$

Taking $I_{\max}$ = 1.1 p.u. for example and i_q = –1.0 p.u. [5], then the steady-state active power range in (8) can be solved at each point of grid voltage $U_g \in [0, 1]$ p.u., as shown in Fig. 4. As the increase of U_g, the range [$P_{e\min}$, $P_{e\max}$] widens. Furthermore, for the case of resistance-inductance grid impedance in Fig. 4(a),

This article has been accepted for publication in a future issue of this journal, but has not been fully edited. Content may change prior to final publication. Citation information: DOI 10.1109/TSTE.2019.2932613, IEEE Transactions on Sustainable Energy

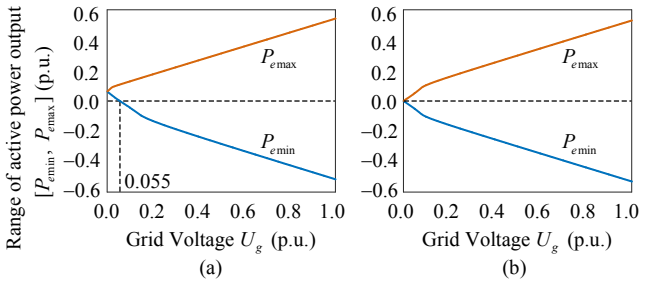

Fig. 4. Steady-state active power output range of a RECS with the change of U_g. (a) Resistance-inductance grid impedance. (b) Pure inductive grid impedance.

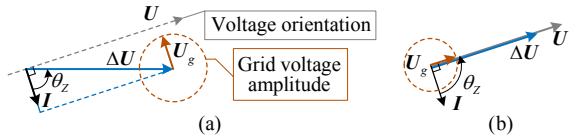

Fig. 5. Existence of equilibrium points when the grid voltage is quite small and active power is zero. (a) There may be no equilibrium point in resistance-inductance grid impedance scenarios. (b) Equilibrium points are certainly existent in pure inductive grid impedance scenarios.

P_{emin} is larger than zero when U_g is smaller than 0.055, for which a physical explanation is made as follows.

Equation (8) yields the steady-state active power output as:

$$P_e = \underbrace{IU_g \cos(\delta + \theta_I)}_{-P_g} + \underbrace{I^2 R_g}_{P_{loss}} \tag{9}$$

where $\theta_I = \arctan(i_q/i_d)$. If $R_g \neq 0$, then both the active and reactive currents will cause some active power loss on this resistive component:

$$P_{loss} = I^2 R_g = I^2 Z \cos\theta_Z = I\Delta U \cos\theta_Z \tag{10}$$

where I is the current amplitude; Z and θ_Z are the impedance magnitude and angle, respectively; $\Delta U = IZ$ is the amplitude of the voltage difference on the grid impedance. The power loss, $P_{loss} = P_e + P_g$, could be compensated by both the power grid and the RECS. If the grid voltage is too low in the case of resistance-inductance grid impedance, P_e has to be positive.

The vector diagram of voltage-oriented control is shown in Fig. 5. The current vector $\boldsymbol{I}$ in Fig. 5(a) lags behind the terminal voltage vector $\boldsymbol{U}$ with 90°, and the RECS accordingly outputs zero active power. The voltage difference $\Delta\boldsymbol{U}$ on the grid impedance leads the current vector $\boldsymbol{I}$ with the impedance angle θ_Z. It can be observed that $\boldsymbol{U} = \Delta\boldsymbol{U} + \boldsymbol{U}_g$ impossibly holds since the grid voltage amplitude U_g is too small. In this case, the maximum active power output from the power grid is

$$P_{g\max} = IU_g \tag{11}$$

which is too small to compensate the power loss owing to

$$U_g < \Delta U \cos\theta_Z. \tag{12}$$

If $P_e = 0$ in this case, there will be no equilibrium point and hence the RECS will not be able to synchronize with the grid. The absence of equilibrium points is essentially because $u_q = 0$ as a basic steady-state condition of voltage-oriented vector control cannot be met. In Fig. 5(b), there is certainly an equilibrium point in the case of pure inductive grid impedance no matter how small U_g is, which is because of zero power loss on the grid impedance.

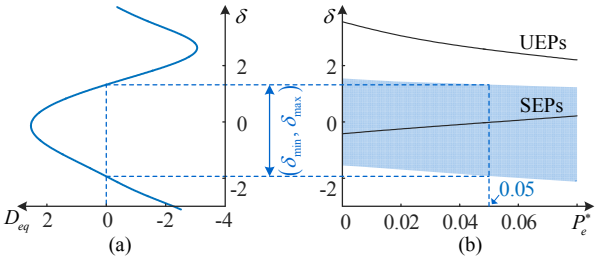

Fig. 6. (a) The curve of $D_{eq}(\delta)$ corresponding to $P_e^* = 0.05$ p.u.. The curve is not an ideal sine/cosine curve since u_d in (13) is also related to δ. (b) The positive damping range (δ_{min}, δ_{max}) slightly changes with P_e^*, where the corresponding stable equilibrium points (SEPs) is within (δ_{min}, δ_{max}) whereas the unstable equilibrium points (UEPs) is outside (δ_{min}, δ_{max}).

From the perspective of equilibrium point, it can be concluded that an appropriate active power reference, which should be set within the steady-state active power output range, is much important for the RECS to possess an equilibrium point after the grid fault.

B. Transient Damping Characteristics

If $D_{eq} > 0$, the role of the damping term in (6) is to achieve negative feedback regulation. For example, if ω_{pll} is larger than ω_g, then the positive damping term is able to contribute a negative change rate of ω_{pll} to facilitate the decrease of ω_{pll}. Hence, a positive damping coefficient is helpful to the transient stability. The damping coefficient D_{eq} (see Appendix) is

$$D_{eq}(\delta) = \frac{-i_q^* k_p U_g \omega_b}{k_i}\left[\cos\delta - \frac{\omega_{pll} L_g P_e^* \sin\delta}{u_d^2 + R_g P_e^*}\right] \tag{13}$$

which is affected by the PLL angle δ, grid voltage U_g, power reference P_e^*, grid impedance, PLL parameters, etc. Generally, the damping effect originates from the proportional unit of the PLL, since if k_p is taken as zero then D_{eq} will become zero. A large k_p along with a small k_i is conducive to the enhancement of the damping effect. The impacts of these circuit parameters and control parameters on the transient stability have been comprehensively investigated in our prior work [16].

In particular, the sign of D_{eq} is determined by δ. There is a range (δ_{min}, δ_{max}) $\in [-\pi, \pi]$ in which $D_{eq} > 0$. When δ is outside the range, the damping effect becomes negative, which endangers the transient stability. Therefore, δ is supposed to lie within the range to maintain a positive damping coefficient,

$$\delta \in (\delta_{min}, \delta_{max}) \tag{14}$$

where δ_{min}, δ_{max} can be calculated by solving $D_{eq}(\delta) = 0$ together with (1) and (5). Fig. 6(a) shows an example of the range, to which the corresponding P_e^* is 0.05 p.u. The positive damping range (δ_{min}, δ_{max}) slightly changes with the active power reference P_e^* as shown in Fig. 6(b). With P_e^* given, the corresponding equilibrium points can be classified into stable equilibrium point (SEP) within the range (δ_{min}, δ_{max}) and unstable equilibrium point (UEP) outside the range (δ_{min}, δ_{max}).

C. Transient Process Analysis

The existence of equilibrium points is a prerequisite for the

This article has been accepted for publication in a future issue of this journal, but has not been fully edited. Content may change prior to final publication. Citation information: DOI 10.1109/TSTE.2019.2932613, IEEE Transactions on Sustainable Energy

transient stability. Even if equilibrium points exist, however, there is a possibility of transient instability due to poor transient behaviors such as too large overshoot and negative damping [13]. The EAC method is often adopted to analyze the transient rotor angle stability of SGs. In view of the mathematical similarity of motion equation, the method is utilized in this study to analyze the transient behaviors of RECSs.

The damping term in SGs' swing equation is neglected in use of the EAC method considering that the damping coefficient of SGs are always positive and relatively small. Things are different for RECSs. One must firstly ensure that $D_{eq} > 0$, i.e., δ is within ($\delta_{\min}$, $\delta_{\max}$), in use of the EAC. Otherwise, the result from the criterion may be overly optimistic. Based on this, one could remove the damping term while using the EAC. Since the amplitude of D_{eq} is significantly larger than J_{eq} (see Appendix), removing the damping term might lead to a conservative criterion. However, this EAC based stability analysis approach itself is extremely useful for transient instability mechanism analysis and parameter sensitivity investigation [16].

By combing (4) and (6), it can be derived that

$$\frac{1}{2}J_{eq}(\omega_{pll}-\omega_g)^2\Big|_{\delta_{0+}}^{\delta_t}=\int_{\delta_{0+}}^{\delta_t}(P_e^*-P_e)d\delta \tag{15}$$

where δ_{0+} is the initial PLL angle after a grid fault occurs. A grid fault often changes the Thévenin equivalent representation of the grid, and accordingly δ also changes [13]. Here the subscript "0+" is used to represent the instantaneous change. δ_t in (15) is the PLL angle at any subsequent time t.

Once P_e^*, i_q^*, and U_g in (7) are given, the active power output $P_e = f(\delta)$ as a function of δ is determined. The power curve is plotted in Fig. 7, where P_{e0+} is the instantaneous active power output corresponding to δ_{0+} at the initial time after a grid fault occurs and δ_{SEP} is the steady-state stable PLL angle corresponding to P_e^*. The PLL angle δ should not exceed the range ($\delta_{\min}$, $\delta_{\max}$) during transient processes. Otherwise, the negative damping effect and even reverse regulation will appear. Note that δ is not equal to the included angle between the terminal voltage and the grid voltage during transient processes [see Fig. 2(b)], and thus δ should not be referred to as the power angle. In this regard, there is a fundamental difference between RECSs and SGs in the transient stability mechanism.

1) $P_e^* > P_{e0+}$

If the given P_e^* during the fault is larger than P_{e0+}, then δ_{SEP} will be larger than δ_{0+}, as shown in Fig. 7(a). In the first period, $P_e^* > P_e$ leads to a continuous increase of ω_{pll} and δ. As a result, P_e increases as well and more active power is outputted to balance with P_e^*. When P_e rises to P_e^* at δ_{SEP}, ω_{pll} reaches the maximum but δ continues increasing because ω_{pll} is larger than ω_g. Afterwards, $P_e^* < P_e$, leads to a decrease of ω_{pll}.

As analyzed above, ω_{pll} will increase in the first period. Based on (15), the accelerating area can be expressed by

$$S_+=\int_{\delta_{0+}}^{\delta_{SEP}}\left(P_e^*-P_e\right)d\delta. \tag{16}$$

Then ω_{pll} decreases in the second period. If the accumulated virtual energy in the PLL cannot be released completely before δ reaches $\delta_{\max}$, then δ will enter the negative damping zone. A conservative analysis is made in this study. The range ($\delta_{\min}$, $\delta_{\max}$) is regarded as the allowable motion range of δ, beyond which

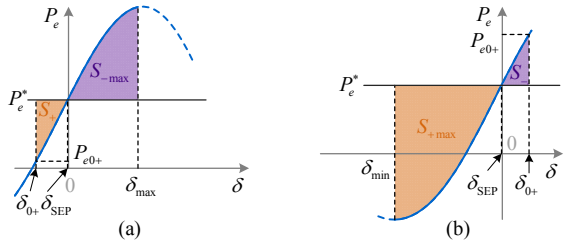

Fig. 7. Illustration of PLL accelerating and decelerating areas. (a) $P_e^* > P_{e0+}$. (b) $P_e^* < P_{e0+}$.

TABLE I
TRANSIENT STABILITY CRITERION

Active power references	Results	Causes
$P_e^* > P_{emax}$	Instable	Without SEPs
$P_e^* < P_{emin}$	Instable	Without SEPs
$P_{emin} \le P_e^* \le P_{emax}$, $P_e^* > P_{e0+}$, $S_+ \le S_{-\max}$	Stable	Eq. (18) holds
$P_{emin} \le P_e^* \le P_{emax}$, $P_e^* < P_{e0+}$, $S_- \le S_{+\max}$	Stable	Eq. (19) holds
Others	Instable [a]	Insufficient buffer

[a] Instable to a large extent rather than certainly instable unless reverse regulation occurs since δ further enters the adjacent reverse regulation zone.

the transient stability cannot be assessed by the EAC any longer. Consequently, the maximum buffer area for decelerating is

$$S_{-\max}=\int_{\delta_{SEP}}^{\delta_{\max}}\left(P_e-P_e^*\right)d\delta. \tag{17}$$

From (16) and (17), the transient stability criterion in this case can be derived as follows,

$$S_+ \le S_{-\max}. \tag{18}$$

2) $P_e^* < P_{e0+}$

If the given P_e^* during the fault is smaller than P_{e0+}, then δ_{SEP} is smaller than δ_{0+}, as shown in Fig. 7(b). The transient stability criterion can be similarly analyzed and derived as

$$S_- \le S_{+\max}. \tag{19}$$

The decelerating area is expressed as

$$S_-=\int_{\delta_{0+}}^{\delta_{SEP}}\left(P_e-P_e^*\right)d\delta. \tag{20}$$

The maximum buffer area for accelerating is described as

$$S_{+\max}=\int_{\delta_{\min}}^{\delta_{SEP}}\left(P_e^*-P_e\right)d\delta. \tag{21}$$

D. Transient Stability Criterion

The transient stability criterion can be finally summarized in Table I, based on which the transient stability can be assessed. Since (7) is much complex, numerical calculation instead of analytical calculation is recommended in the stability assessment. Note that the transient stability cannot be judged strictly once the PLL angle δ exceeds the maximum buffer area and enters the negative damping zone. If δ further enters the adjacent reverse regulation zone, the transient instability would be undoubted. Table I suggests again that an appropriate active power reference is crucial to the transient stability.

IV. TRANSIENT STABILITY ENHANCEMENT METHOD

The LOS during grid faults easily leads to RECSs' tripping. A great deal of RECSs' tripping endangers the power system stability. To address the transient instability risk associated with the LOS, three typical stability enhancement methods

This article has been accepted for publication in a future issue of this journal, but has not been fully edited. Content may change prior to final publication. Citation information: DOI 10.1109/TSTE.2019.2932613, IEEE Transactions on Sustainable Energy

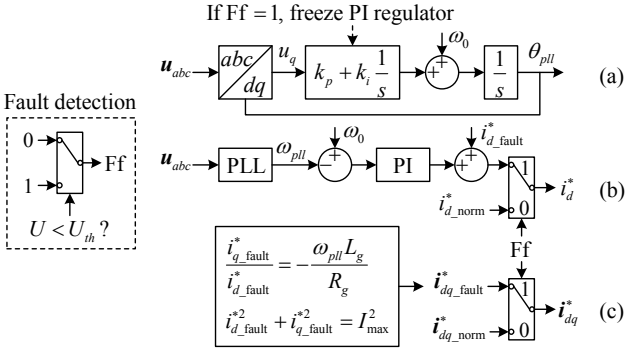

Fig. 8. Three existing typical transient stability enhancement methods. (a) PLL freezing method [10]. (b) PLL frequency based method [11]. (c) Adaptive current injecting method [13].

TABLE II
PROS AND CONS OF SEVERAL STABILITY ENHANCEMENT METHODS

Methods	Refs	Pros	Cons
PLL freezing method	[10]	Easy-to-use	Static error exists
PLL freq. based method	[11]	Easy-to-use	Stability without theoretical proof
ACI method	[13]	Stable even zero voltage	Need post-fault impedance estimation
Proposed method	NA	Stable and easy-to-use	Maybe less reactive power outputted

have been developed in [10], [11] and [13], as depicted in Fig. 8. The simplest method is the PLL freezing method [10], [27], which freezes the proportional-integral (PI) regulator of PLL during grid faults. The PLL frequency (freq.) based method [11] regulates the active current reference according to the detected frequency. The adaptive current injecting (ACI) method [13] specifies the ratio of active and reactive current references according to the post-fault equivalent grid impedance. Though these methods possess some advantages as shown in Table II, they are insufficient to some extent because of the disadvantages shown in the last column. To this end, this study proposes a novel transient stability enhancement method, which is based on dynamic active power balance.

According to the developed stability criterion, the active power reference should be set within the steady-state active power output range. Besides, the decelerating or accelerating area in the first period should be reduced as far as possible in order to avoid entering the negative damping zone in the second period. Due to the occurrence of the grid voltage sags after grid faults occur, the active power output would drops to a certain value P_{e0+}. Ideally, if the active power reference is set to the real-time measured active power P_{e0+}, then the accelerating or decelerating area in the first period could be minimized as far as possible. Considering that it is easy to measure the active power output at the RECS terminal, the active power reference can be set to the measured active power output during grid faults. With this consideration, the motion equation (6) becomes

$$\begin{aligned} &J_{eq}\, d\omega_{pll}/dt + D_{eq}\left(\omega_{pll}-\omega_g\right)=0 \\ &d\delta/dt=\omega_b\left(\omega_{pll}-\omega_g\right). \end{aligned} \tag{22}$$

Equation (22) indicates that the system would be stable if $D_{eq} \geq 0$, unstable if $D_{eq} < 0$. Recalling (13), it suggests that $D_{eq} \geq 0$

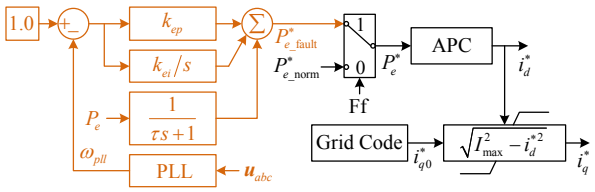

Fig. 9. Proposed transient stability enhancement method, where 1.0 is the per-unit rated frequency intended for approximately representing the actual grid frequency. The fault flag "Ff": 0 – Normal mode, 1 – Fault mode.

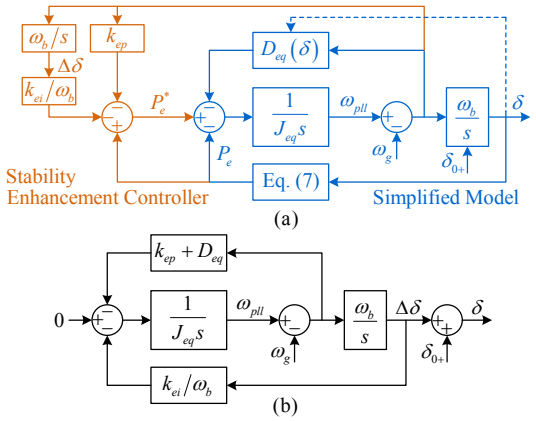

Fig. 10. (a) System model diagram with the transient stability enhancement method incorporated, where $\Delta\delta$ is the state variable of the integral regulator. (b) Rearranging the model to the simplest form, which is similar to the form of the Phillips-Heffron model of SGs.

cannot be guaranteed since D_{eq} probably becomes negative with δ. To ensure positive damping effect, it is necessary to compensate the damping coefficient. Moreover, (22) shows that δ is another crucial state variable besides ω_{pll}. Hence, it is necessary to keep δ within the closed-loop control system.

For these two purposes, a PI regulator is adopted to regulate the frequency deviation. As shown in Fig. 9, the active power reference during grid faults is given by

$$\begin{aligned} P^*_{e\_fault} &= P_e+\left(k_{ep}+k_{ei}/s\right)\left(\omega_g-\omega_{pll}\right) \\ &\approx P_e+\left(k_{ep}+k_{ei}/s\right)\left(1.0-\omega_{pll}\right) \end{aligned} \tag{23}$$

where k_{ep} and k_{ei} are the gains of the PI regulator. In view of the difficulty of fast measurement of the grid frequency ω_g in (23), it is approximately represented by the rated frequency i.e., 1.0. In spite of the approximation, it is still able to improve the damping effect and the approximation is acceptable in engineering practice. Furthermore, a low-pass filter is utilized to filter harmonics in the output active power P_e in order to avoid harmonic instability, as shown in Fig. 9.

The system model with the stability enhancement method incorporated is depicted in Fig. 10(a), which is further rearranged to the simplest form in Fig. 10(b). It is interesting to notice that the form is similar to the Phillips-Heffron model of SGs [28]. This similarity again illustrates the roles of the proportional regulator and the integral regulator, i.e., to regulate the frequency deviation (i.e., enhance the damping effect) and to regulate the PLL angle deviation. The model shown in Fig. 10(b) is described by

This article has been accepted for publication in a future issue of this journal, but has not been fully edited. Content may change prior to final publication. Citation information: DOI 10.1109/TSTE.2019.2932613, IEEE Transactions on Sustainable Energy

$$J_{eq}\, d\omega_{pll}/dt + \left(k_{ep} + D_{eq}\right)\left(\omega_{pll} - \omega_g\right) + k_{ei}\Delta\delta/\omega_b = 0$$
$$d\Delta\delta/dt = \omega_b\left(\omega_{pll} - \omega_g\right) \tag{24}$$

where $\Delta\delta$ denotes the state variable of the integral regulator [see Fig. 10(a)]. The transient stability enhancement method is disabled until grid faults occur, which suggests that the initial value of $\Delta\delta$ is zero. In addition, (24) implies that $\Delta\delta$ converges to zero at the steady state while ω_{pll} converges to ω_g.

A. Steady-State Performance Analysis

After a grid fault occurs at the time t_0, the PLL angle's initial value at t_{0+} is denoted as δ_{0+}, as done in Section III. The relationship between δ_t and $\Delta\delta_t$ at any time t can be obtained:

$$\delta_t = \delta_{0+} + \omega_b \int_{0+}^{t} \left(\omega_{pll} - \omega_g\right) d\tau = \delta_{0+} + \Delta\delta_t \tag{25}$$

where the initial value of $\Delta\delta$ is zero. Given that $\Delta\delta$ converges to zero at the steady state, δ accordingly converges to its initial value δ_{0+} at the steady state according to (25), i.e.,

$$\delta_s = \delta_{0+}. \tag{26}$$

With the steady-state value δ_s, the steady-state active current i_d can be calculated from (5). Further, the steady-state active power output can be calculated from (9), i.e.,

$$P_e = I_{\max} U_g \cos(\delta_s + \theta_I) + I_{\max}^2 R_g. \tag{27}$$

B. Transient Performance Analysis

While neglecting the grid frequency dynamics, rearranging the system model (24) yields the second-order differential equation:

$$J_{eq}\, d^2\Delta\delta/dt^2 + \left(k_{ep} + D_{eq}\right) d\Delta\delta/dt + k_{ei}\Delta\delta = 0. \tag{28}$$

The transient performance of the proposed method as well as the influences of the gain parameters on the performance can be easily assessed by thinking of (28) as a typical second-order system. For assuring asymptotic stability, requirements are made on the gain parameters:

$$\begin{cases} k_{ep} + D_{eq} > 0 \\ k_{ei} \geq 0. \end{cases} \tag{29}$$

For analyzing the transient performance, the damping ratio ξ and the natural frequency ω_n are derived:

$$\xi = \left(k_{ep} + D_{eq}\right) \Big/ \left(2\sqrt{k_{ei} J_{eq}}\right),\ \omega_n = \sqrt{k_{ei}/J_{eq}} \tag{30}$$

which indicates that the damping ratio is improved with the increase of k_{ep} and decrease of k_{ei}. A large damping ratio is beneficial for the transient stability. However, too large damping ratio could lead to too long setting time. For $\xi > 0.69$, the setting time can be approximately estimated by [29]

$$t_s \approx 4.5\xi/\omega_n = 2.25\left(k_{ep} + D_{eq}\right)/k_{ei} \tag{31}$$

which suggests that a large k_{ep} as well as a small k_{ei} makes the setting time long.

C. Parameter Tuning

Considering both the stability requirement in (29) and the setting time in (31), there should be a tradeoff in the tuning of k_{ep}. Once k_{ep} is tuned, k_{ei} can be tuned according to (30) by taking $\xi = 0.707$ which is a commonly used damping ratio in engineering practice. Following this guideline, k_{ep} is set to 5 in this study considering that a typical damping coefficient D_{eq} during severe grid faults is about within the range [–3.1, 2.5], as shown in Appendix. Then k_{ei} is set within the range (80, 150), and the setting time is accordingly about 0.1 s. For actual applications, the method of trial and error combined with the guideline is still recommended. Besides, the bandwidth of the low-pass filter should be smaller than the switching frequency but larger than the bandwidth of (28). The filtering time constant τ is finally set to 0.01 s.

The proposed transient stability enhancement method is supposed to be activated after a grid fault and deactivated once the grid fault clearance is detected. The resynchronization of the RECS with the grid after the fault clearance is assuring because the normal grid voltage amplitude facilitates sufficient buffer areas and a quite large positive damping coefficient.

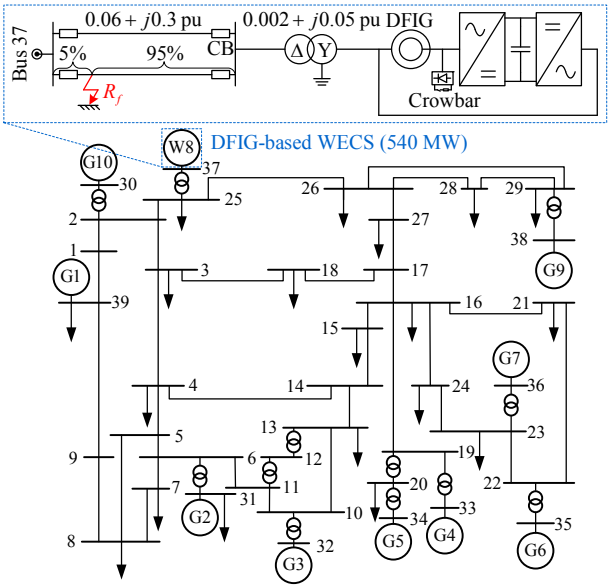

Fig. 11. Network topology of the New England 39-bus test system, in which the capacity base of the WECS is 540 MVA.

TABLE III
DFIG'S PARAMETERS (PART)

Parameters	Per-unit values	Parameters	Per-unit values
Stator resistance	0.008	RSC inner loop k_p	1.2
Stator leakage inductance	0.171	RSC inner loop k_i	50
Rotor resistance	0.006	PLL k_p	200
Rotor leakage inductance	0.156	PLL k_i	2000
Mutual inductance	2.9	Fig. 9, k_{ep}	5
Turbine inertia constant	5.0 s	Fig. 9, k_{ei}	100
Grid coupling inductance	0.3	Fig. 9, τ	0.01

V. SIMULATION RESULTS

To obtain realistic responses and credible results, the RECS in simulations is connected to the New England 39-bus test system instead of the infinite bus, as shown in Fig. 11. Since the SG on the Bus 37 in the original test system outputs almost zero reactive power in the steady state, replacing it by a RECS with the same capacity and unity-power factor control has little effect on the steady-state power flow. The RECS is specifically

This article has been accepted for publication in a future issue of this journal, but has not been fully edited. Content may change prior to final publication. Citation information: DOI 10.1109/TSTE.2019.2932613, IEEE Transactions on Sustainable Energy

modeled as a doubly-fed induction generator (DFIG) based WECS, and the verification on other RECSs with full-scale power converters can be made similarly. The simulations are performed on the PSCAD/EMTDC, where the power converter is modeled with switch-level accuracy and the SGs are equipped with exciter and governor. Partial critical DFIG's parameters are summarized in Table III.

It has been known from Table I that there are two types of transient instability. The one is that there is no SEP during grid faults. The other is that the maximum buffer area is insufficient though SEPs exist, accordingly leading the operating point to enter the negative damping zone and even adjacent reverse regulation zone. To separately produce these two types of instability scenarios and evaluate the effectiveness of the proposed transient stability enhancement method, two cases are simulated, which are Case A: transient instability without SEPs and Case B: transient instability due to insufficient buffer area.

A. Transient Instability Without SEPs

A three-phase line-to-ground fault occurs at 0.2 s and the grounding resistance R_f in this case is 0.01 Ω. Then the voltage at Bus 37 dips to about 0.06 p.u. which is so small that there is no SEP after the fault. Fig. 12 shows the simulation result with the conventional method where the active power reference is zero during the fault. The WECS enters the LVRT Stage I, in which the crowbar circuit is activated to suppress the transients. Subsequently (~30 ms), the crowbar circuit is deactivated, the control function of the rotor-side converter is regained and the WECS enters the LVRT Stage II. As shown in Fig. 12(b) and (f), the reactive current reference and active power reference are set to –1 p.u. and 0.0 p.u., respectively. Fig. 12(e) indicates that the PLL frequency gradually deviates from the rated frequency until reaching the limit 0.8 p.u. In other words, the WECS cannot resynchronize with the grid during the LVRT Stage II. Fig. 12(f) shows that the active power reference is smaller than its actual value during the transient process, and therefore the PLL frequency decreases, which coincides with the theoretical analysis. Moreover, there are harmonics in the output current and also in the terminal voltage due to the frequency difference between the WECS and the power grid. In practice, the LOS would lead to the tripping of the WECS.

The fault line is disconnected at 0.6 s by opening the circuit breakers (CBs) on this line. At this time, both the grid voltage and the terminal voltage returns to near the rated voltage, as shown in Fig. 12(a). Fig. 12(e) displays that the WECS can resynchronize with the power system again after the terminal voltage recovery. After the fault is cleared at 1.0 s, the condition of successful reclosure is met. The CBs are accordingly reclosed at 1.2 s. The grid impedance is instantly reduced by half, which introduces a minor disturbance to the system.

The LOS in Fig. 12(e) during the fault is due to there is no SEP, which is caused by zero active power reference. From the circuit point of view, the reactive current produces active power loss $i_q^2 R_g$ on the grid impedance (resistive component), but the grid voltage is too low to completely compensate the active power loss. Therefore, the WECS is supposed to output some active power in order to avoid the transient instability.

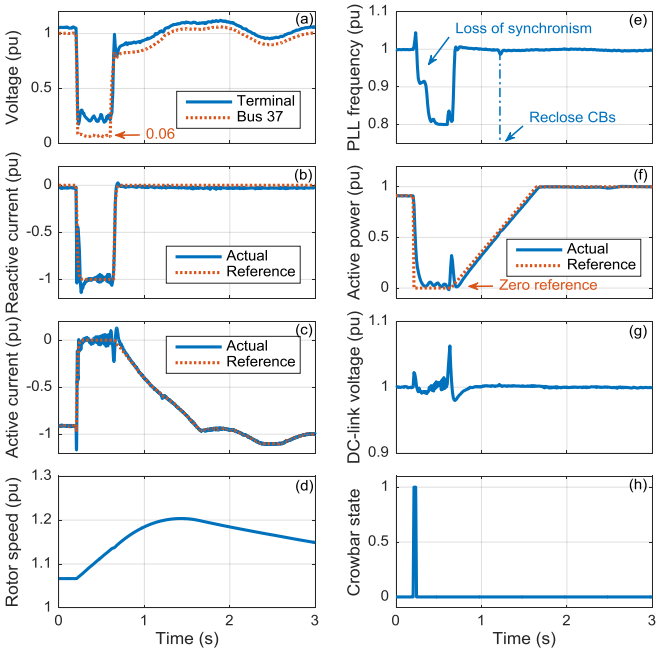

Fig. 12. Simulation result of Case A with the conventional method. The residual grid voltage is so small that there is no SEP, and hence the PLL cannot resynchronize with the grid. Note the sudden increase of the PLL frequency at the fault time is due to the phase jump of the grid voltage [27].

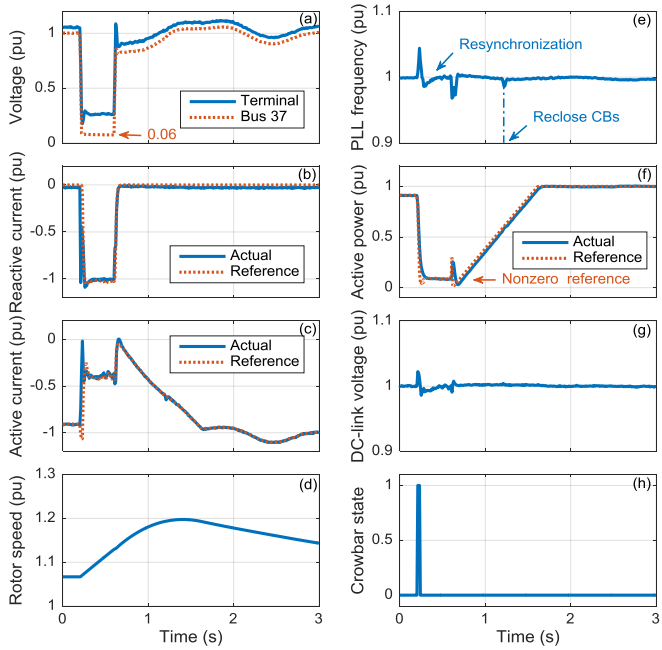

Fig. 13. Simulation result of Case A with the proposed method, where an active power reference larger than zero is generated, and hence the PLL is able to resynchronize with the grid after the fault.

The simulation result with the proposed method enabled is shown in Fig. 13. A nonzero active power reference is generated automatically during the fault by the additional control loop, as shown in Fig. 13(f). Hence, the active power reference is balanced with its actual value. Fig. 13(e) indicates that the PLL frequency returns to the rated one immediately once the active power balance is achieved. Since the current limit I_{max} is

This article has been accepted for publication in a future issue of this journal, but has not been fully edited. Content may change prior to final publication. Citation information: DOI 10.1109/TSTE.2019.2932613, IEEE Transactions on Sustainable Energy

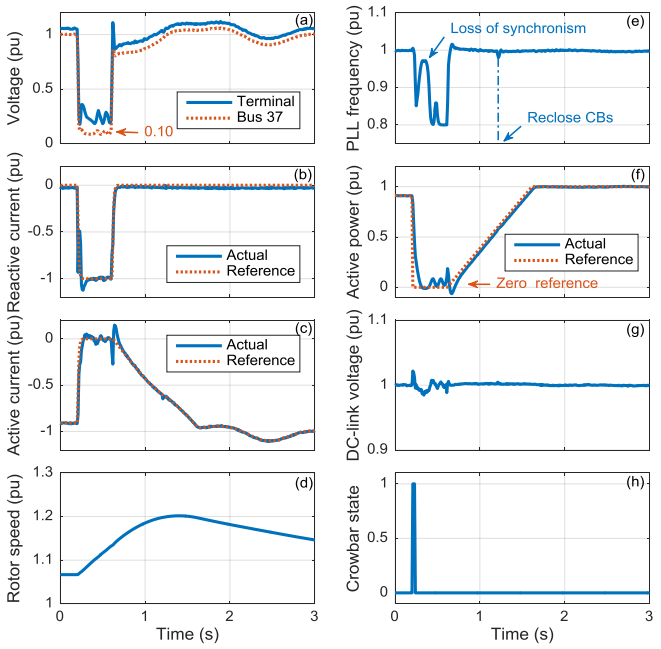

Fig. 14. Simulation result of Case B with the conventional method. The voltage at Bus 37 dips to about 0.10 p.u. that is larger than that in Case A. Therefore there is indeed a SEP after the fault, but the PLL is still not able to resynchronize with the grid since the buffer area for accelerating is not enough.

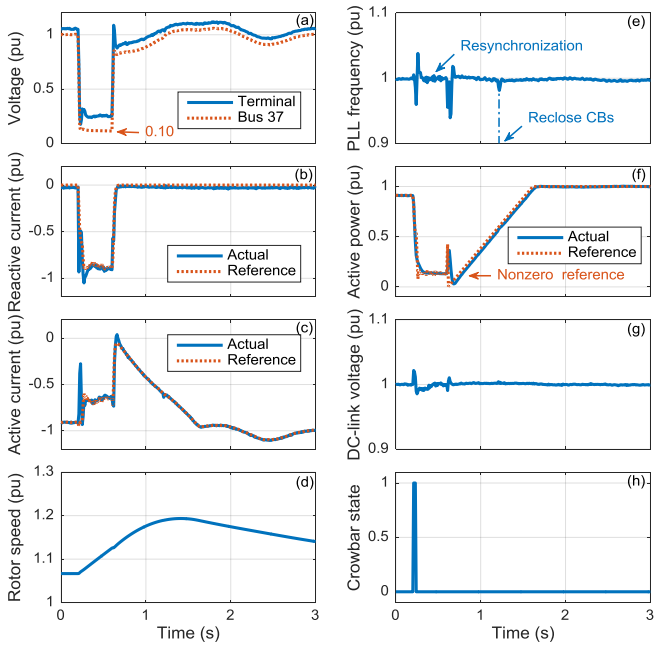

Fig. 15. Simulation result of Case B with the proposed method, where the PLL is able to resynchronize with the grid after the fault.

set to 1.1 p.u., the reactive current can still reach 1.0 p.u. though additional active current is outputted in the meantime.

B. Transient Instability Due to Insufficient Buffer Area

The grounding resistance R_f in this case is 0.04 Ω. The fault is not severer than that in Case A. It can be verified that the post-fault SEP certainly exists in this case. Figs. 14 and 15 show the simulation results with the conventional method and the proposed method, respectively. The transient response in this case is similar to that in Case A. The main difference lies in that the voltage at Bus 37 dips to about 0.10 p.u, which is slightly larger than that in Case A. Hence, there is indeed a SEP after the fault. Nonetheless, Fig. 14(e) shows that the PLL still fails to resynchronize with the residual grid voltage. Referring to the analysis in Fig. 7(b), the decelerating area in this case is too large to match the maximum buffer area for accelerating due to a zero active power reference that is not appropriate. Fig. 14(e) shows that the first swing of the PLL fails to reach the rated frequency, which demonstrates again that the accelerating area is insufficient. The consequent negative damping effect and the reverse regulation in the adjacent decelerating zone are the root cause of the transient instability.

In Fig. 15, a nonzero active power reference is generated automatically by the proposed method, as shown in Fig. 15(f). Fig. 15(e) shows that the PLL successfully resynchronizes with the residual grid voltage. Besides, the damping effect is enhanced and hence the PLL frequency overshoot is suppressed.

The voltage, frequency, active power and reactive power of several buses are displayed in Fig. 16. It shows that the voltage sag at Bus 37 and the generation loss from the WECS (Bus 37) have a large effect on the entire power system. Since the generators are not equipped with power system stabilizer (PSS), the system takes a longer time to enter the steady state.

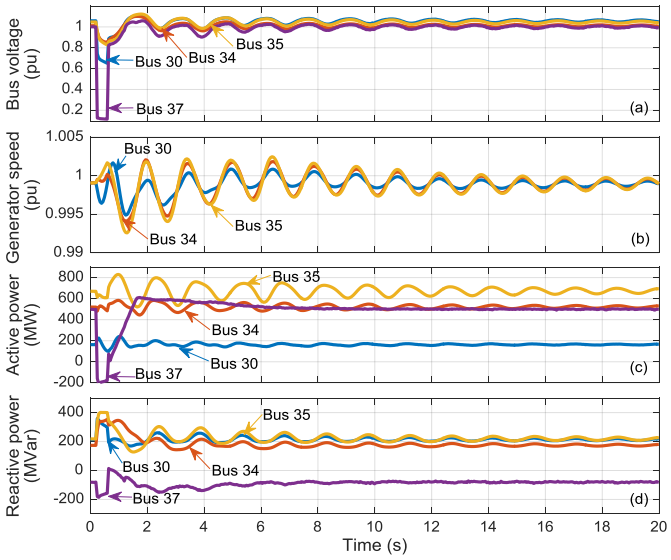

Fig. 16. Bus 30, Bus 34, Bus 35, and Bus 37 voltage, frequency, active power and reactive power in Case B simulation.

C. Comparisons with State-of-the-Art Methods

The proposed transient stability enhancement method is also compared with three state-of-the-art methods in Table II. Fig. 17 shows all the methods address the LOS issue by outputting positive instead of zero active power. Both the proposed method and the PLL frequency based method [11] show high performance in terms of small overshoot, fast convergence and zero static error. However, the stability of the latter method [11] has not been theoretically proven yet.

For the PLL freezing method, the frozen PLL can no longer

This article has been accepted for publication in a future issue of this journal, but has not been fully edited. Content may change prior to final publication. Citation information: DOI 10.1109/TSTE.2019.2932613, IEEE Transactions on Sustainable Energy

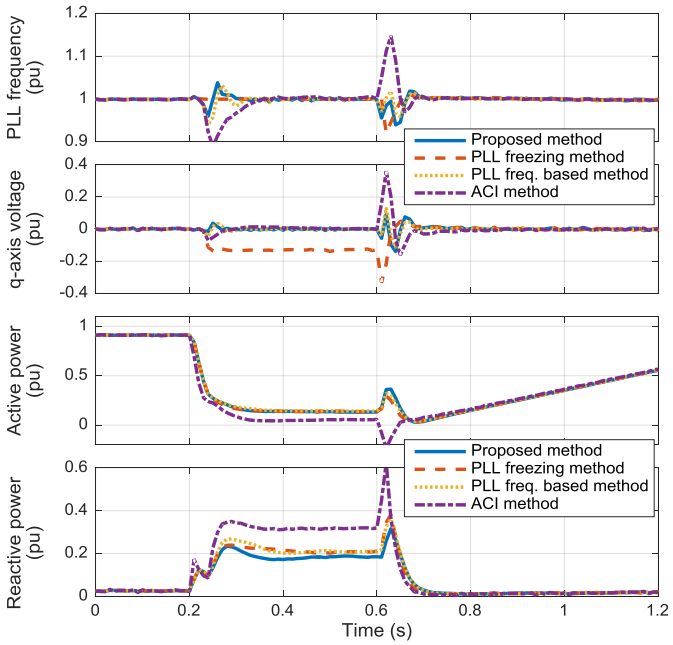

Fig. 17. Comparisons with other methods, where the proposed method shows high performance in terms of overshoot and convergence speed.

detect the post-fault terminal voltage phase-angle which undergoes a jump at the moment of the fault [27]. Consequently, there is a static error in the PLL freezing method (see the steady-state q-axis voltage). It should be noted that the static error may cause the reactive power injection ($-u_d i_q + u_q i_d$) to be negative, which would have a negative impact on the grid voltage. In spite of this defect, this method is recommended by North American Electric Reliability Corporation (NERC) to address the LOS issue [30], probably considering that the self-stability of RECSs takes precedence over grid-supportive functions. By contrast, the proposed method in this study could be regarded as a potentially practical method for transient stability enhancement.

VI. Conclusions

It is challenging for grid-connected RECSs to resynchronize with the power grid after extremely severe grid voltage sags. This paper describes RECS' transient responses during LVRT with a novel swing equation model to study the transient stability mechanism and criterion, where the unbalanced power term is the difference between the reference and output of active power. Based on the model, it is found that there is a transient instability possibility due to the interaction between the PLL and the terminal voltage, in which the active power output is also affected by both. The comprehensive analysis shows that, the transient stability during severe grid voltage sags can be maintained when the following two conditions are satisfied: 1) the active power reference is set within the range of steady-state active power output so that there is an equilibrium point; 2) the equal area criterion is satisfied on the premise that the PLL angle lies within the positive damping zone. It is clarified from the transient mechanism and criterion that an appropriate active power reference is crucial to the transient stability. Hence a dynamic active power balance based transient stability enhancement method is proposed, evaluated and verified.

It should be noted that negative-sequence voltage components appear when asymmetrical faults occur, and thus advanced PLLs should be adopted. Our future work will address the transient stability and resynchronization issues involving advanced PLLs coping with asymmetrical faults.

Acknowledgement

Bikash C. Pal's activity has been supported by the U.K.–China initiative in Stability and Control of Power Networks with Energy Storage (STABLE-NET) funded by Research Councils U.K. (RCUK) Energy Programme in U.K. (Contract EP/L014343/1).

Appendix

A. Guideline for PLL Parameter Tuning

It is known the small-signal model of the synchronous reference frame PLL (SRF-PLL) [31] in the per-unit system is

$$\left(\theta-\theta_{pll}\right)\left(k_p+k_i/s\right)/s=\theta_{pll} \tag{A.1}$$

which yields the transfer function:

$$\theta_{pll}/\theta=\left(k_p s+k_i\right)/\left(s^2+k_p s+k_i\right). \tag{A.2}$$

Hence, the PLL bandwidth can be calculated as follows,

$$f_{bw}=\sqrt{k_p^2+2k_i+\sqrt{k_p^4+4k_p^2k_i+8k_i^2}}\Big/\left(2\sqrt{2}\pi\right)(\text{Hz}). \tag{A.3}$$

The small-disturbance damping ratio of the SRF-PLL is

$$\xi_{pll}=k_p/\left(2\sqrt{k_i}\right). \tag{A.4}$$

For RECSs, typical PLL bandwidth f_{bw} is about within the range 20~40 Hz while the damping ratio ξ_{pll} could be tuned within 0.7~2.0 for enhanced damping effect of the entire system. The parameters can be chosen within an empirical range in advance and then check them with (A.3) and (A.4).

The PLL parameters in this study are chosen as 200, 2000, and thus the PLL bandwidth is about 33 Hz while the damping ratio is roughly 2.2. Even though the small-disturbance damping ratio of the PLL itself is large enough, the entire system is still likely to become unstable after large-disturbance grid faults. A detailed analysis has been made in Section III.

B. Derivation of the Equivalent Swing Equation

From (1) and (5), it can be obtained that

$$\begin{aligned} u_d&=U_g\cos\delta+R_g P_e^*/u_d-\omega_{pll}L_g i_q^* \\ u_q&=-U_g\sin\delta+R_g i_q^*+\omega_{pll}L_g P_e^*/u_d \end{aligned} \tag{A.5}$$

which give rise to

$$\frac{du_d}{dt}=-U_g\sin\delta\omega_b\left(\omega_{pll}-\omega_g\right)-\frac{R_g P_e^*}{u_d^2}\frac{du_d}{dt}-L_g i_q^*\frac{d\omega_{pll}}{dt} \tag{A.6}$$

$$\frac{du_q}{dt}=-U_g\cos\delta\omega_b\left(\omega_{pll}-\omega_g\right)+\frac{L_g P_e^*}{u_d}\frac{d\omega_{pll}}{dt}-\frac{\omega_{pll}L_g P_e^*}{u_d^2}\frac{du_d}{dt}. \tag{A.7}$$

Substituting (A.6) into (A.7) obtains the expression of du_q/dt. Then, substituting it into (2) gives rise to the expression of $d\omega_{pll}/dt$. Further, consider that

$$P_e^*-P_e=-u_q i_q^* \tag{A.8}$$

where $P_e^*=u_d i_d^*$ and $P_e=u_d i_d+u_q i_q\approx u_d i_d^*+u_q i_q^*$. Using (A.8)

This article has been accepted for publication in a future issue of this journal, but has not been fully edited. Content may change prior to final publication. Citation information: DOI 10.1109/TSTE.2019.2932613, IEEE Transactions on Sustainable Energy

and rearranging the expression of $d\omega_{pll}/dt$ yields that

$$J_{eq}\, d\omega_{pll}/dt = P_e^* - P_e - D_{eq}\left(\omega_{pll} - \omega_g\right) \tag{A.9}$$

$$\begin{aligned} J_{eq} &= \frac{-i_q^*\omega_b}{k_i}\left(1 - \frac{k_p L_g P_e^*}{u_d\omega_b} - \frac{k_p\omega_{pll}L_g^2 P_e^* i_q^*}{\left(u_d^2 + R_g P_e^*\right)\omega_b}\right) \\ D_{eq} &= \frac{-i_q^* k_p U_g\omega_b}{k_i}\left[\cos\delta - \frac{\omega_{pll}L_g P_e^*\sin\delta}{u_d^2 + R_g P_e^*}\right] \triangleq D_{eq}\left(\delta\right). \end{aligned} \tag{A.10}$$

In fact, the motion of the PLL is directly driven by its input variable u_q. Equation (A.8) establishes the relationship between u_q and the active power deviation, hence suggesting that the motion of the PLL can be driven equivalently by the active power deviation, as mathematically described by (A.9). Equation (A.9) has mathematic meaning only if i_q^* is not zero. Otherwise, $P_e^* \approx P_e$ always holds. For this reason, (A.9) is developed mainly to analyze LVRT conditions and $i_q^* \neq 0$ is its application condition.

Taking the simulation Case B as an example, the per-unit inertia and damping coefficients during the grid fault can be approximately calculated:

$$J_{eq} \approx \frac{-i_q^*\omega_b}{k_i} \approx 0.16,\ D_{eq} \approx -0.3 + 2.8\cos\left(\delta + 0.14\right) \tag{A.11}$$

The response of the PLL is fast and accordingly J_{eq} is quite small. Additionally, the intention in PLL parameter tuning is almost no overshoot allowed, and hence the amplitude of D_{eq} is large enough. Unfortunately, the damping coefficient affected by δ may become negative. These characteristics distinguish RECSs from SGs in transient responses after grid faults.

REFERENCES

[1] J. Yao, L. Guo, T. Zhou, D. Xu, and R. Liu, "Capacity configuration and coordinated operation of a hybrid wind farm with fsig-based and pmsg-based wind farms during grid faults," *IEEE Trans. Energy Convers.*, vol. 32, no. 3, pp. 1188–1199, Sep. 2017.

[2] H. Geng, C. Liu, and G. Yang, "LVRT capability of DFIG-based WECS under asymmetrical grid fault condition," *IEEE Trans. Ind. Electron.*, vol. 60, no. 6, pp. 2495–2509, Jun. 2013.

[3] S. Xiao, G. Yang, H. Zhou, and H. Geng, "An LVRT control strategy based on flux linkage tracking for DFIG-based WECS," *IEEE Trans. Ind. Electron.*, vol. 60, no. 7, pp. 2820–2832, Jul. 2013.

[4] M. Firouzi and G. B. Gharehpetian, "LVRT Performance Enhancement of DFIG-Based Wind Farms by Capacitive Bridge-Type Fault Current Limiter," *IEEE Trans. Sustain. Energy*, vol. 9, no. 3, pp. 1118–1125, Jul. 2018.

[5] E. O. N. Netz, "Grid code-high and extra high voltage," E. ON Netz GmbH, Bayreuth, Apr. 2006.

[6] J. Hu, B. Wang, W. Wang, H. Tang, Y. Chi, and Q. Hu, "Small signal dynamics of DFIG-based wind turbines during riding through symmetrical faults in weak ac grid," *IEEE Trans. Energy Convers.*, vol. 32, no. 2, pp. 720–730, Jun. 2017.

[7] J. Z. Zhou, H. Ding, S. T. Fan, Y. Zhang, and A. M. Gole, "Impact of short-circuit ratio and phase-locked-loop parameters on the small-signal behavior of a VSC-HVDC converter," *IEEE Trans. Power Del.*, vol. 29, no. 5, pp. 2287–2296, Oct. 2014.

[8] J. Hu, Y. Huang, D. Wang, H. Yuan, and X. Yuan, "Modeling of Grid-Connected DFIG-Based Wind Turbines for DC-Link Voltage Stability Analysis," *IEEE Trans. Sustain. Energy*, vol. 6, no. 4, pp. 1325–1336, Oct. 2015.

[9] J. Liu, W. Yao, J. Wen, J. Fang, L. Jiang, H. He, and S.-J. Cheng, "Impact of Power Grid Strength and PLL Parameters on Stability of Grid-Connected DFIG Wind Farm," *IEEE Trans. Sustain. Energy*, pp. 1–1, 2019.

[10] B. Weise, "Impact of K-factor and active current reduction during fault-ride-through of generating units connected via voltage-sourced converters on power system stability," *IET Renew. Power Gener.*, vol. 9, no. 1, pp. 25–36, Jan. 2015.

[11] Ö. Göksu, R. Teodorescu, C. L. Bak, F. Iov, and P. C. Kjær, "Instability of wind turbine converters during current injection to low voltage grid faults and PLL frequency based stability solution," *IEEE Trans. Power Syst.*, vol. 29, no. 4, pp. 1683–1691, Jul. 2014.

[12] D. Dong, B. Wen, D. Boroyevich, and P. Mattavelli, "Analysis of phase-locked loop low-frequency stability in three-phase grid-connected power converters considering impedance interactions," *IEEE Trans. Ind. Electron.*, vol. 62, no. 1, pp. 310–321, Jan. 2015.

[13] S. Ma, H. Geng, L. Liu, G. Yang, and B. C. Pal, "Grid-synchronization stability improvement of large scale wind farm during severe grid fault," *IEEE Trans. Power Syst.*, vol. 33, no. 1, pp. 216–226, Jan. 2018.

[14] H. Geng, L. Liu, and R. Li, "Synchronization and reactive current support of PMSG based wind farm during severe grid," *IEEE Trans. Sustain. Energy*, vol. 9, no. 4, pp. 1596–1604, Oct. 2018.

[15] S. Ma, H. Geng, G. Yang, and B. Liu, "Experimental validation of adaptive current injecting method for grid-synchronization improvement of grid-tied REGS during short-circuit fault," in *Proc. IPEC-Niigata*, 2018.

[16] X. He, H. Geng, and S. Ma, "Transient stability analysis of grid-tied converters considering PLL's nonlinearity," *CPSS Trans. Power Electron. Appl.*, vol. 4, no. 1, pp. 40–49, Mar. 2019.

[17] H. Wu and X. Wang, "Design-oriented transient stability analysis of grid-connected converters with power synchronization control," *IEEE Trans. Ind. Electron.*, vol. 66, no. 8, pp. 6473–6482, Aug. 2019.

[18] H. Wu and X. Wang, "Transient stability impact of the phase-locked loop on grid-connected voltage source converters," in *Proc. IPEC-Niigata*, 2018.

[19] H. Wu and X. Wang, "An adaptive phase-locked loop for the transient stability enhancement of grid-connected voltage source converters," in *Proc. IEEE ECCE*, 2018.

[20] M. G. Taul, X. Wang, P. Davari, and F. Blaabjerg, "An overview of assessment methods for synchronization stability of grid-connected converters under severe symmetrical grid faults," *IEEE Trans. Power Electron.*, pp. 1–1, 2019.

[21] Z. Shuai, C. Shen, X. Liu, Z. Li, Z. J. Shen, "Transient angle stability of virtual synchronous generators using Lyapunov's direct method," *IEEE Trans. Smart Grid*, pp. 1–1, 2018.

[22] M. Kabalan, P. Singh, and D. Niebur, "Nonlinear Lyapunov stability analysis of seven models of a DC/AC droop controlled inverter connected to an infinite bus," *IEEE Trans. Smart Grid*, vol. 10, no. 1, pp. 772–781, Jan. 2019.

[23] G. Han, C. Zhang, and X. Cai, "Mechanism of frequency instability of full-scale wind turbines caused by grid short circuit fault and its control method," *Trans. of China Electrotechnical Society*, vol. 33, no. 10, pp. 2167–2175, 2018.

[24] Q. Hu, L. Fu, F. Ma, and F. Ji, "Large signal synchronizing instability of PLL-based VSC connected to weak AC grid," *IEEE Trans. Power Syst.*, pp. 1–1, 2019.

[25] M. Zhang, X. Yuan, and J. Hu, "Inertia and primary frequency provisions of PLL-synchronized VSC HVDC when attached to islanded AC system," *IEEE Trans. Power Syst.*, vol. 33, no. 4, pp. 4179–4188, Jul. 2018.

[26] W. He, X. Yuan, J. Hu, "Inertia provision and estimation of PLL-based DFIG wind turbines", *IEEE Trans. Power Syst.*, vol. 32, no. 1, pp. 510–521, Jan. 2017.

[27] M. G. Taul, X. Wang, P. Davari, and F. Blaabjerg, "Grid Synchronization of Wind Turbines during Severe Symmetrical Faults with Phase Jumps," *Proc. IEEE ECCE*, 2018.

[28] S. Tan, H. Geng, G. Yang, H. Wang, and F. Blaabjerg, "Modeling framework of voltage-source converters based on equivalence with synchronous generator," *J. Modern Power Syst. Clean Energy*, Jul. 2018.

[29] B. C. Kuo, "Transient response of a prototype second-order system," in *Automatic Control Systems*, 9th ed. Upper Saddle River: Prentice Hall, 1995, ch. 5, sec. 6, pp. 275–288.

[30] Joint NERC and WECC Staff Report, "900 MW Fault Induced Solar Photovoltaic Resource Interruption Disturbance Report – Southern California Event: October 9, 2017," Feb. 2018, [Online]. Available: www.nerc.com.

[31] S.-K. Chung, "A phase tracking system for three phase utility interface inverters," *IEEE Trans. Power Electron.*, vol. 15, no. 3, pp. 431-438, May 2000.

This article has been accepted for publication in a future issue of this journal, but has not been fully edited. Content may change prior to final publication. Citation information: DOI 10.1109/TSTE.2019.2932613, IEEE Transactions on Sustainable Energy

Xiuqiang He (S'17) received the B.S. degree in Department of Automation, Tsinghua University, Beijing, China, in 2016. He is currently working toward the Ph.D. degree at Department of Automation, Tsinghua University.

His current research interests include synchronization stability of power converters interfaced generation systems, and dynamic equivalent modeling of large-scale wind power plants.

Mr. He was a recipient of the Chinese National Scholarship, and the IEEE International Power Electronics and Application Conference and Exposition (PEAC) Excellent Paper Award in 2018.

Hua Geng (S'07–M'10–SM'14) received the B.S. degree in electrical engineering from Huazhong University of Science and Technology, Wuhan, China, in 2003, and the Ph.D. degree in control theory and application from Tsinghua University, Beijing, China, in 2008.

From 2008 to 2010, he was a Postdoctoral Research Fellow with the Department of Electrical and Computer Engineering, Ryerson University, Toronto, ON, Canada. He joined the Department of Automation, Tsinghua University, in June 2010, where he is currently an Associate Professor. His current research interests include advanced control of power electronics and renewable energy conversion systems.

Dr. Geng serves as an editor of IEEE Trans. Energy Conversion, an associate editor of IEEE Trans. Industry Applications and an associate editor of Chinese Journal of Electrical Engineering.

Ruiqi Li received the B.E. degree in mechatronics engineering from Beijing Institute of Technology, Beijing, China, in 2010, the M.E. degree in mechatronics engineering from the University of Chinese Academy of Sciences, Beijing, China, in 2013, and the Ph.D. degree in control theory and application from Tsinghua University, Beijing, China, in 2017.

He joined China Electronics Standardization Institute in July 2017. His research focuses on grid integration problems of renewable energy conversion systems.

Bikash C. Pal (M'00–SM'02–F'13) received the B.E.E. (Hons.) degree from Jadavpur University, Kolkata, India, in 1990, the M.E. degree from the Indian Institute of Science, Bangalore, India, in 1992, and the Ph.D. degree from Imperial College London, London, U.K., in 1999, all in electrical engineering.

He is currently a Professor with the Department of Electrical and Electronic Engineering, Imperial College London. His research interests include state estimation and power system dynamics.

He is Vice President Publications, IEEE Power and Energy Society. He was Editor in-Chief of IEEE Transactions on Sustainable Energy (2012-2017) and Editor in-Chief of IET Generation, Transmission and Distribution (2005-2012) and is a Fellow of IEEE for his contribution to power system stability and control.